AIAA

A02-13981

AIAA 2002-0482

THE STUDY OF THE TURBULENT BURNING VELOCITY BY IMAGING THE WRINKLED FLAME SURFACE

Sergei A. Filatyev, James F. Driscoll
Department of Aerospace Engineering
University of Michigan
Ann Arbor, MI 48109-2140

Campbell D. Carter
Innovative Scientific Solutions, Inc.
Dayton, OH 45440

Jeffrey M. Donbar
Air Force Research Laboratory, AFRL/PRA
Wright-Patterson AFB, OH 45433

40th Aerospace Sciences Meeting & Exhibit
11-14 January 2002 / Reno, NV

The Study of the Turbulent Burning Velocity by Imaging the Wrinkled Flame Surface

Sergei A. Filatyev[1], James F. Driscoll[1],
Campbell D. Carter[2] and Jeffrey M. Donbar[3]

[1]Department of Aerospace Engineering, University of Michigan, Ann Arbor 48109
[2]Innovative Scientific Solutions, Inc., Dayton OH 45440
[3]Air Force Research Laboratory, AFRL/PRA, Wright-Patterson AFB OH 45433

Abstract The nonlinear dependence of the turbulent burning velocity ($\overline{S}_T$) on the mean velocity and the turbulence intensity level was studied. The goal was to determine if the burning velocity curve has nonlinear "bending" as turbulence intensity level increases and to study reasons why the nonlinear behavior exists. A new and unambiguous way to measure ($\overline{S}_T$) was developed. It requires proper measurements of the total mass flow rate of reactants and the correct area of the time-averaged flame surface. A stoichiometric methane-air slot burner with 2-D mean flow and surrounding outer flames was used. Mean velocity was varied in the range from 3 to 12 m/s and turbulent intensity level was varied in the range from 5 to 25%. Images of the wrinkled flame surface were recorded.

It was found that nonlinear "bending" behavior does occur. Mean velocity was found to be a governing parameter in addition to turbulent intensity level. To understand the flame merging, strain, and possible extinction processes that can contribute to the "bending" phenomenon, turbulent eddies were identified as they cross the wrinkled flame surface using simultaneous CH-PLIF/PIV diagnostics.

The CH layer images show that flame surface loss by local extinction does not occur, and thus is not a cause of the "bending" observed. Instead, the merging of flame fronts is observed to create loss of flame area at high turbulence levels; thus flamelet merging is shown to be one cause of the 'bending' phenomenon.

Introduction

The first goal of this work is to define, in an unambiguous way, a characteristic global turbulent burning velocity, denoted $\overline{S}_T$, for one fundamental type of premixed flame geometry, and to report a set of measured $\overline{S}_T$ values that can be used to assess numerical simulations. A second goal is to investigate reasons for the observed non-linear relation between $\overline{S}_T$ and the incident velocity fluctuations (u') which has been denoted "bending" and has been reported in several previous studies [1-11]. A motivation for this work is the fact that new laser-light sheet diagnostics now provide accurate images of the instantaneous flame boundary, which are needed to properly determine the turbulent burning velocity.

The present study quantifies the global turbulent burning velocity for one particular geometry: a 2-D Bunsen flame. It is argued that this is one of the "canonical" flames for which the global burning velocity $\overline{S}_T$ can be defined unambiguously. To avoid ambiguity the total mass per second of reactants consumed within a well-defined flame area must be known. The 2-D configuration avoids ambiguities associated with conical (axisymmetric) bunsen flames; conical flames oscillate across the laser sheet, which results in the underestimation of the flame height. The global burning velocity is defined as:

$$\overline{S}_T = m_R \ / \ (\rho_R \ \overline{A}_{FLAME}) \qquad (1)$$

where m_R is the total mass flow of reactants into the entire flame, and $\overline{A}_{FLAME}$ is the area of the time-averaged flame surface. An advantage of using the burning velocity defined by Eq. 1 is that local velocities do not have to be measured, and streamlines do not have to be defined, which have complicated some previous studies. To measure $\overline{S}_T$ it is important that all of the reactants pass through the flame sheet, which occurs for the 2-D slot bunsen flame

It is recognized that the values of $\overline{S}_T$ which are reported below are valid only for this 2-D slot burner geometry and only should be used to assess numerical simulations of this particular geometry. However, experimental evidence now indicates that for any experiment, the global and local burning

velocities are valid only for that particular geometry. Both depend on the degree of flame wrinkling, as quantified by the flame surface density (Σ), which depends not only on the local turbulence levels, but on the entire flame geometry, including the boundary conditions [5, 7, 12, 13, 14]. This indicates that a "universal" relation between S_T and u' does not exist. Instead, it is important for models to correctly include boundary conditions in order to simulate Σ, which can be done using direct numerical simulation or the Coherent Flamelet Model [7].

The "bending" of the burning velocity relation between S_T and u' for this geometry was investigated. This nonlinear behavior has been measured by Bradley [1] and others [2-6] and has been predicted by various models [7-11]. It is physically reasonable to expect "bending" to occur as the turbulence level is increased sufficiently. The flame surface area cannot grow indefinitely, for several reasons. (a) Merging of flame segments reduce the surface area, as is predicted by the sink term in the Σ equation [7, 13]. (b) Gas expansion creates divergent velocity fields that prevent segments from becoming too densely packed. (c) Large strain rates [1] eventually will decrease the local stretched laminar burning velocity. (d) Local extinction eventually should reduce the flame area. The fact that "bending" has not been observed in some experiments may indicate that the turbulence level was not sufficiently large for that particular geometry.

Experimental Arrangement

The 2-D slot bunsen burner shown in Fig. 1 was selected for several reasons. First, a conical bunsen flame has a problem in that the cone tip oscillates in the direction normal to a laser sheet that often is used to estimate the area $\overline{A}_{FLAME}$ in Eq. 1. When the cone tip is not in the sheet, the height of the true conical flame is much larger than the height of the image in the light sheet. Light sheet measurements for a cone can greatly underpredict $\overline{A}_{FLAME}$ and thus overpredict $\overline{S}_T$. The slot burner avoids this problem. All of the reactants must pass through the flame; none are diverted around it.

The central burner shown in Fig. 1 consists of a 25 mm by 50 mm slot through which a stoichiometric methane-air mixture flows. Three identical burners were used which provided turbulence intensities (u'/$\overline{U}$) at the burner exit that were approximately 5%, 10% and 20%, respectively, by employing different grids and a layer of metal spheres. A laser velocimeter was used to measure exact values of (u'/$\overline{U}$). The mean velocities chosen were 3, 5, 8 and 12 m/s, which were determined from the total mass flowrate of reactants, that was measured using calibrated choked orifices. It is important to eliminate disturbances from any undesirable shear layer that may occur where the product gases contact the ambient room air. To do so, the two outer burners shown in Fig. 1 were used. They are 25 mm by 50 mm slots upon which grids are placed to stabilize many very short Meeker-burner flames (2 mm high). These short flames provide streams of product gas that are nearly equal in velocity to the product gas from the main flame. The outer burners also are operated with a stoichiometric methane-air mixture.

The diagnostics used to image the flame boundary were simultaneous planar laser-induced fluorescence (PILF) of the CH radical -and particle-image velocimetry (PIV) ; [15 and 16] as well as Mie scattering from micron-sized oil drops. In brief, for the PLIF measurements, the output of a Nd:YAG-pumped dye laser operating at 616 nm was frequency mixed with residual fundamental output from the Nd:YAG laser, generating 390-nm radiation. This laser system was then tuned to the $Q_1(7.5)$ transition of the B-X(0,0) band of CH. An intensified CCD camera (Roper PI-MAX) fitted with a Nikon 58-mm f/1.2 lens (and Schott KV418 and BG1 filters) was then employed to capture fluorescence, principally from the A-X bands in the 420-440 nm region. The PIV system includes two frequency-doubled Continuum Surelite Nd:YAG lasers and a double-frame CCD camera with 2K by 2K resolution (the Redlake ES4.0). PIV images were acquired with an Epix framegrabber and software (XCAP), while timing of the lasers and cameras was accomplished using a Quantum Composer delay generator. The fields of view for both cameras were 35-mm-square (both sides of the flame were imaged), and these fields were aligned using a custom target manufactured on a 1-mm-thick fused-silica plate. For PIV 0.5-micron alumina flakes were seeded into the reactants so that velocities could be measured in both hot and cold portions of the flow. Commercial LaVision PIV software—employing multiple passes and the interrogation region offsetting technique—was applied to attain a resolution of 0.3-mm (the size of the interrogation region on the final pass), equating to a 16-pixel region on the ES4.0 CCD. For the Mie-scattering measurements, however, micron-sized PD-23 oil drops were employed along with a high-resolution (3K by 2 K) Kodak 460 digital camera. Again, a frequency-doubled Nd:YAG was employed as the light source.

The area $\overline{A}_{FLAME}$ in Eq. 1 is defined as a surface area of a triangular prism that has the same

3

American Institute of Aeronautics and Astronautics

average height, length and width as the 2-D slot flame. To determine the average flame height, the laser sheet cross-sectional images were used. The average flame height is $2\overline{A}_{SHEET}/L$. The quantity $\overline{A}_{SHEET}$ is the averaged area of the reactants that is imaged in a laser-sheet cross sectional image of the flame. These two quantities are related by:

$$\overline{A}_{FLAME} = W\,L\,[(4\,\overline{A}_{SHEET}/L^2)^2 + 1]^{1/2} \qquad (2)$$

L is the burner length and W is the width, as indicated in Fig. 1.

Results

Figure 2 summarizes the values of global burning velocities $\overline{S}_T$ that were measured using the light-sheet images and Eqs. 1 and 2. Each data point was determined from 70 images obtained at each of twelve test conditions. The four mean velocities were 3, 5, 8, and 12 m/s, and the nominal turbulence levels $(u'/\overline{U})$ were 5%, 10%, and 20%. The dashed line represents a curvefit to some previous measurements that were made in conical bunsen flames [17-20]. From the arguments presented above, there is no reason to expect agreement between the 2-D slot bunsen flame data and the conical flame data because of geometrical differences that affect wrinkling. However the dashed line is shown to illustrate that the present values lie below the conical flame data. This difference may be due to the fact that the cone tip oscillates out of the plane of the laser sheet, so measurements of the height of a 3-D conical flame may be erroneously low, leading to erroneously large values of $\overline{S}_T$. The differences, however, may only be due to geometric differences.

Fig. 2 shows that the mean velocity $\overline{U}$ is an important parameter for this geometry, and that if $\overline{U}$ is held constant and u' is varied independently, the curves in Fig. 2 display a nonlinear "bending" character. Non-linear effects begin to occur for values of u'/S_L in the range from 2 to 4 for this experiment, based on the data in Fig. 2. This range appears to be similar to the range in which similar curves begin to bend for other flame geometries [1-6].

Figure 3 shows how the perimeter (P_T) of the wrinkled flame surface varies as u' is increased, while holding $\overline{U}$ constant. For each laser sheet image, the flame boundary was identified and an algorithm was developed to correctly determine the perimeter of this wrinkled boundary. The average perimeter of 70 images is P_T. Then the boundaries for the 70 images were superimposed and the average flame boundary was determined; the perimeter of this average boundary is P_A. Values of $(P_T/P_A)^2$ provide a qualitative, but not quantitative, measure of the ratio of the area of the wrinkled flame to the unwrinkled case, which has been predicted to be equal to S_T/S_L in the flamelet regime. Figure 3 shows that flame wrinkledness displays a nonlinear bending behavior that is similar to that seen in Fig. 2. Again, if a curve was drawn through the rightmost triangle, square, and diamond in Fig. 2, the resulting curve would not bend, indicating that $\overline{U}$ must be fixed for the curves in Fig. 3 to bend.

Figures 4-7 are instantaneous snapshots of the CH layer and the vorticity field. They are presented in order to investigate, in a qualitative sense only, if the area of the present flame may be reduced by the extinction, pocket burning, and merging processes that are predicted by Eq. 3. A highly turbulent condition is selected for which $\overline{S}_T$ is no longer in the linear regime; $\overline{U}$ is 8 m/s, $u'/\overline{U}$ is 0.20, u'/S_L is 4.4. The thick line in Figures 4-7 represents the CH layers, within which CH fluorescence signal exceeds 10% of its maximum value. The large eddies are shown as red and blue regions, within which the vorticity magnitude exceeds 2000 /s. Note that there is a marked decrease in the number of large eddies (per area) as the eddies are forced to cross the flame boundary. This is consistent with the observation that the vorticity of single vortex is severely reduced as it crosses a flame [21], due to viscous effects, gas expansion, and baroclinic torques. It also is noted that the CH layer thickness varies by about a factor of two, which may be attributable to stretch effects, but it rarely exceeds one millimeter. The white regions in Figs. 4 and 5 are regions where the PIV seeding particle density is insufficient (the outer flames were not seeded) so velocity measurements were not possible.

Figures 4-7 show that the flame boundary is continuous; there are no locations along the layers where the CH signal decreases to the noise level. So it is concluded that local flame extinction is not a possible reason for the nonlinear behavior seen in Figs. 2 and 3. Numerous pockets of reactants are seen in Figs. 4-6. The large turbulence levels cause the flame boundary to become highly wrinkled, so thin "neck" regions are seen. Flame area will be reduced due to the merging of flames in the neck regions, and due to the inward burning of reactants in the pockets. For example, the CH layers shown in Fig. 6b were imaged 100 msec after the layers seen in Fig. 6a, and the flame area is observed to be significantly less at the later time. Note that the neck region in the upper right of Fig. 6a is about to burn through and that a pocket of reactants appears at this location in Fig. 6b. The time resolution of 100 ms is

4

not sufficient to allow quantitative conclusions to be drawn about flame merging. However, the images do show that the degree of flame merging, necking, and inward burning of pocket is much larger, in a qualitative sense, for flames in the "bending" regime than for those at lower values of u'/S_L (Fig. 8).

Figures 7a and 7b show examples of counter-rotating eddy pairs which exert compressive and extensional strain on the flame. These are magnified views of the regions denoted A and B in Fig. 4. To better visualize the rotating velocity pattern, constant horizontal and vertical velocity components were subtracted from each velocity vector in the PIV images. Note that in Fig. 7a the flame is pulled into the region between the two eddies, imparting a large curvature to the CH layer. In theory, a purely compressive strain field should reduce the flame area, since negative strain exerts a negative stretch rate; however, the eddies in Fig. 7a are affecting both the strain rate and the curvature, and it is likely that the flame area would increase if the CH layer was advected in the direction of the velocity vectors. In Fig. 7b the eddy pairs exert extensional (positive) strain, similar to that of a counterflow geometry. Note that the CH layer is thinner between the two eddies. Figure 8 shows a region where the density of eddies is especially large. This is a segment of the boundary that was shown in Fig. 5. The large number of eddies is seen to create intense wrinkling of the surface, although no extinction is seen. There are many eddies in the products, but they are significantly smaller than those in the reactants.

Conclusions

1. A global turbulent burning velocity was defined in an unambiguous way, and was measured for a simple flame that can be numerically modeled

2. Bending of the burning velocity relation is observed if u' (the r.m.s. velocity fluctuation level) is varied independently, while keeping mean velocity fixed.

3. The mean velocity has a strong effect on the turbulent burning velocity; this effect has not been considered in previous theories.

4. Flame perimeter follows a trend similar to S_T relation.

5. Images of the CH layers show that local extinction does not occur and cannot explain the "bending" phenomenon. The images show that pocket burning and flamelet merging do occur, and the resulting loss of flame surface area may be a cause of the "bending" phenomenon.

6. It was demonstrated that CH-PLIF/PIV

diagnostics allow one to observe pairs of eddies that exert positive and negative strain on the flame. This can affect the surface area and the local burning velocity; however additional research is required to quantify these strain effects.

References
1. Bradley, D., *Proc. Combust. Inst.* 24: 247-262 (1992).
2. Abdel-Gayed, R.G., Bradley, D., Lawes, M., Proc. R. Soc. Lond A414: 389-413 (1987).
3. Abdel-Gayed, R.G., Bradley, D., Hamid, M.N., Lawes, M., *Proc. Combust. Inst.* 20: 505-512 (1984).
4. Shy, S.S., Lin, W.J., and Peng, K.Z., *Proc. Combust. Inst.* 28: 561-568 (2000).
5. Bourguignon, E., Kostiuk, L.W., Michou, Y., and Gokalp, I., *Proc. Combust. Inst.* 26: 447-453 (1996).
6. Karpov, V., Lipatnikov, A., and Zimont, V., *Proc. Combust. Inst.* 26: 249-257 (1996).
7. Duclos, J.M., Veynante, D., and Poinsot, T., *Combust. Flame* 95:101-117 (1993).
8. Peters, N., *J. Fluid Mech.* 348: 107-132 (1999).
9. Aldredge, R.C., *Combust. Flame* 90: 121-133 (1992).
10. Denet, B., *Combust. Theory Model.* 3: 585-589 (1999).
11. Beretycki, H., and Sivashinsky, G.I., SIAM J. Appl. Math 51 (2): 344-350 (1991).
12. Bedat, B., and Cheng, R.K., *Combust. Flame* 100: 485-494 (1995).
13. Candel, S.M.,and Poinsot, T.J., *Combust. Sci. Technol.* 70: 1-15 (1990).
14. Paul, R.N., and Bray, K.N.C., *Proc. Combust. Inst.* 26: 259-266 (1996).
15. Donbar, J.M., Driscoll, J.F., and Carter, C.D., *Combust. Flame* 125: 1239-1257 (2001).
16. Carter, C.D., Donbar, J.M., and Driscoll, J.F., *Appl. Physics B* 66:129-132 (1998).
17. Cheng, R.K., Shepherd, I.G. and Talbot, L., *Proc. Combust. Inst.* 22: 771-780 (1988).
18. Smallwood, G.J., Gulder, O.L., Snelling, D.R., Deschamps, B.M., and Gokalp, I., *Combust. Flame* 101: 461-470 (1995).
19. Yoshida, A. and Gunther, R. , *Combust. Flame*

5

38:249-258 (1980).

20. Kobayashi, H., Tamura, T., Maruta, K., Niioka, T. and Williams, F.A., *Proc. Combust. Inst.* 26: 389-396 (1996).

21. Mueller, C.J., Driscoll, J.F., Reuss, D.L., Drake, M.C., and Rosalik, M.E., *Combust. Flame* 112: 342-358 (1998).
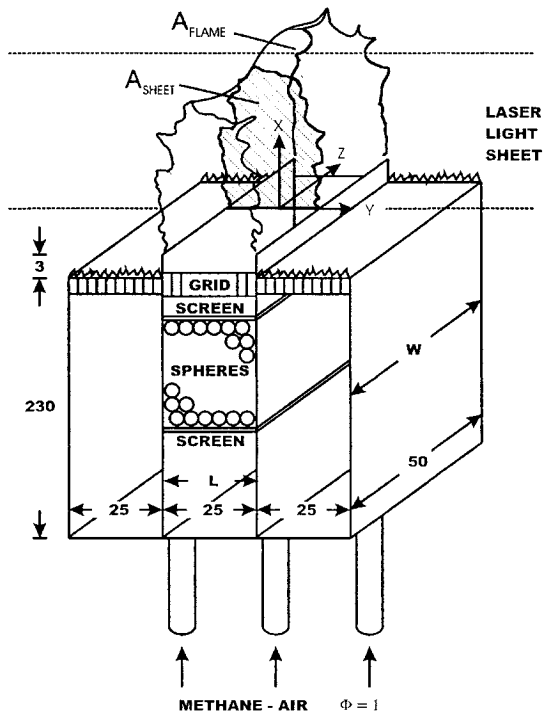
American Institute of Aeronautics and Astronautics

Figure 1. Schematic of the 2-D Slot Bunsen Flame. Dimensions are in mm. The two outer burners eliminate any undesirable disturbances to the flame from shear layers at the product-air interface.
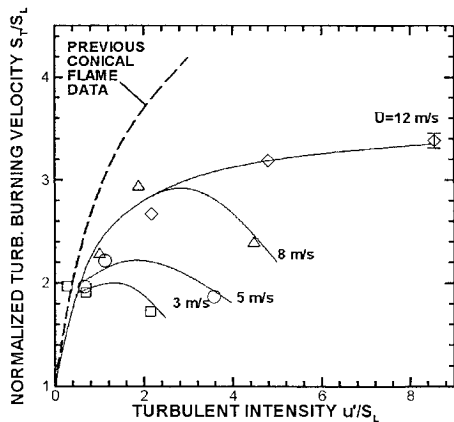

Figure 2. Measured Global Turbulent Burning Velocity $\overline{S}_T$ for the 2-D Slot Bunsen Flame. Stoichiometric methane-air. For each curve, mean velocity $\overline{U}$ was held fixed. Dashed line is a fit to local burning velocities for stoichiometric methane-air flames of Refs. 19-22.
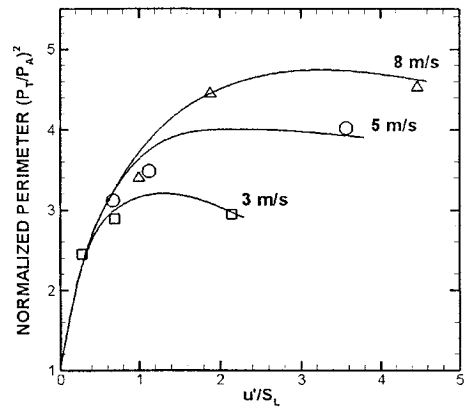
Figure 3. Square of the Normalized Perimeter of the Wrinkled Flame, From Laser Light Sheet Images.
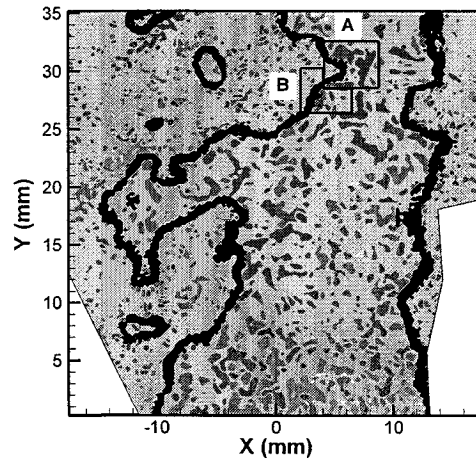
Figure 4. Image of Turbulent Premixed Flame Boundary and Turbulent Eddies. Stoichiometric methane-air, $\overline{U}= 8$ m/s, $u'/\overline{U} = 0.20$. CH layers shown as black lines; red = vorticity magnitude exceeding 2000/s , inducing counterclockwise rotation; blue = vorticity magnitude exceeding 2000/s , inducing clockwise rotation.
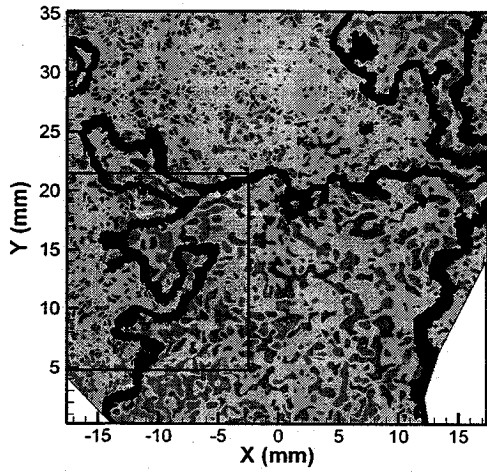
7

Figure 5.   Image of Turbulent Premixed Flame Boundary and Turbulent Eddies. Conditions same as Fig. 4.

Figure 6.   Image of Turbulent Premixed Flame Boundary (CH Layers) at two times. Conditions same as Fig. 4.
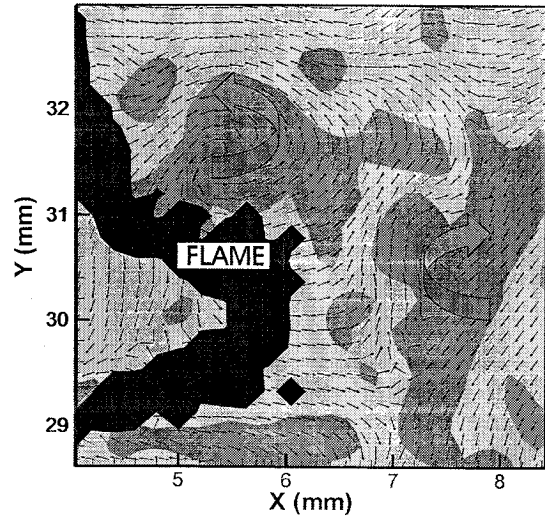

Figure 7a.   Two Adjacent Counterrotating Eddies Which Exert Strain on the Premixed Turbulent Flame. Compressive (negative) strain field in Region A of Fig. 4; Black region is CH layer. Red, blue regions with vorticity magnitude exceeding 2000/s. Velocity vectors from PIV data.
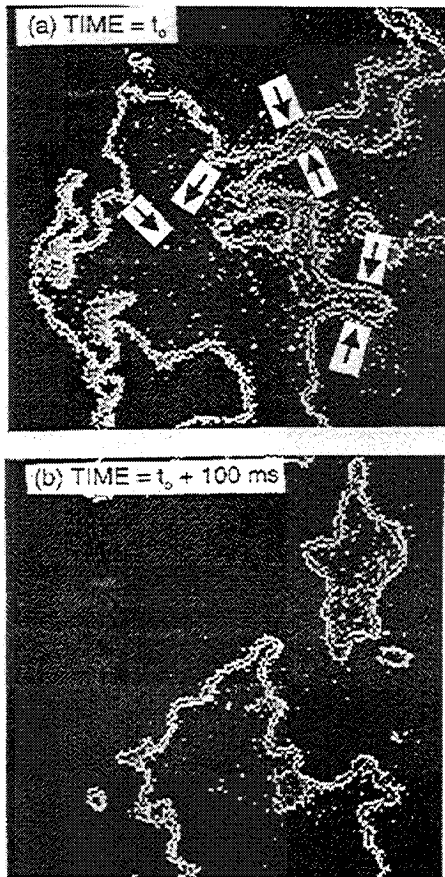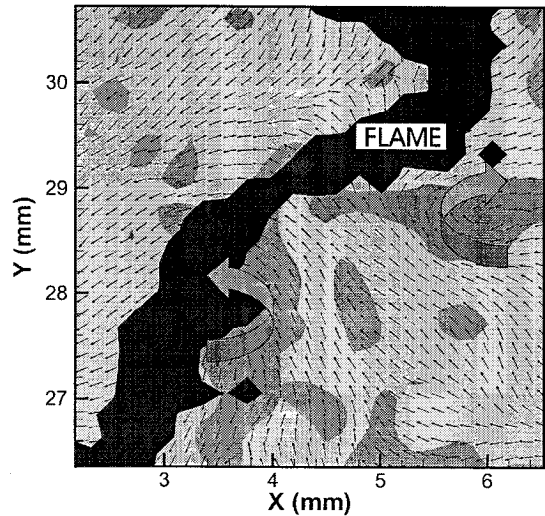

Figure 7b.   Two Adjacent Counterrotating Eddies Which Exert Strain on the Premixed Turbulent Flame. Extensional (positive) strain field in Region B of Fig. 4. Black region = CH layer. Red, blue regions with vorticity magnitude exceeding 2000/s. Velocity vectors from PIV data.
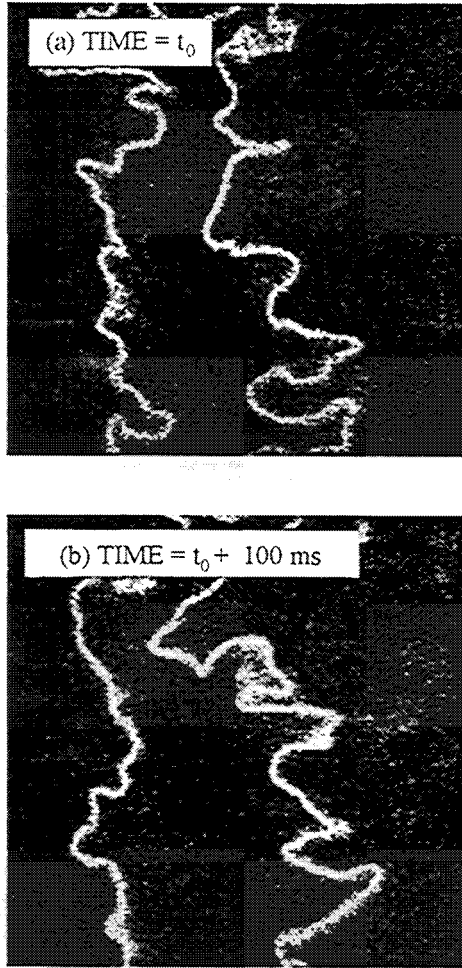
American Institute of Aeronautics and Astronautics

Figure 8.   Image of Turbulent Premixed Flame Boundary (CH Layers) at two times for $\overline{U} = 8$ m/s, $u'/\overline{U} = 0.05$

American Institute of Aeronautics and Astronautics